Article

Theoretical Study on Ethylene Polymerization Catalyzed by Half-Titanocenes Bearing Different Ancillary Groups

Yang Li [1,2], Xiaoling Lai [1], Xiaowei Xu [1], Yat-Ming So [3], Yijing Du [1], Zhengze Zhang [1] and Yu Pan [1,2,*]

[1] School of Chemical Engineering, Dalian University of Technology, Panjin 124221, China; chyangli@dlut.edu.cn (Y.L.); xiaolinglaidut@163.com (X.L.); xuxiaowei2021@163.com (X.X.); duyj7879@163.com (Y.D.); ZhangZhengze@mail.dlut.edu.cn (Z.Z.)

[2] State Key Laboratory of Fine Chemicals, School of Chemical Engineering, Dalian University of Technology, Dalian 116024, China

[3] Department of Chemistry, The Hong Kong University of Science and Technology, Clear Water Bay, Kowloon, Hong Kong, China; chsym@connect.ust.hk

[*] Correspondence: ypan@dlut.edu.cn

Abstract: Half-titanocenes are well known to show high activity for ethylene polymerization and good capability for copolymerization of ethylene with other olefins, and the ancillary ligands can crucially affect the catalytic performance. In this paper, the mechanisms of ethylene polymerization catalyzed by three half-metallocenes, $(\eta^5\text{-}C_5Me_5)TiCl_2(O\text{-}2,6\text{-}^iPr_2C_6H_3)$ (**1**), $(\eta^5\text{-}C_5Me_5)TiCl_2(N=C^tBu_2)$ (**2**) and $[Me_2Si(\eta^5\text{-}C_5Me_4)(N^tBu)]TiCl_2$ (**3**), have been investigated by density functional theory (DFT) method. At the initiation stage, a higher free energy barrier was determined for complex **1**, probably due to the presence of electronegative O atom in phenoxy ligand. At the propagation stage, front-side insertion of the second ethylene is kinetically more favorable than back-side insertion for complexes **1** and **2**, while both side insertion orientations are comparable for complex **3**. The energy decomposition showed that the bridged cyclopentadienyl amide ligand could enhance the rigidity of the active species as suggested by the lowest deformation energy derived from **3**. At the chain termination stage, β-H transfer was calculated to be a dominant chain termination route over β-H elimination, presumably owing to the thermodynamic perspective.

Keywords: ethylene polymerization; DFT; half-titanocene; reaction mechanism

1. Introduction

Since the discovery of Ziegler–Natta and Phillips catalysts in 1950s, polyolefins, mainly consisting of polyethylene (PE) and polypropylene (PP), have become the largest class of commercial thermoplastics, making the polyolefin industry a multibillion-dollar business [1]. Although the industrial application predominantly employs heterogeneous transition metal catalysts, a large number of homogeneous catalysts have been developed for olefin polymerization in both industry and academia [2–4]. Well-defined molecular catalysts can precisely control the catalytic activity as well as modify the molecular weight, molecular weight distribution, comonomer incorporation, and the microstructure of the polyolefin by tailoring the coordination environment of the metal center [5,6]. The modification of ligand generally gives clear feedback to the catalytic performance of the transition metal catalysts. Moreover, it is beneficial to investigate the polymerization mechanism thanks to their well-defined molecular structures and homogeneous reaction conditions [7,8].

With the development of half-metallocene and "constrained-geometry configuration" (CGC) catalysts [9,10], non-bridged half-metallocene catalysts containing anionic ancillary ligands, such as phenoxy [11,12], ketamide [13,14], phosphinimide [15,16], and so on [17], have been exploited and applied in ethylene, styrene, and α,ω-dienes (co)polymerization [18,19]. Remarkable catalytic activities were observed in the ethylene polymerization catalyzed by

the non-bridged half-titanocenes to produce PE with high molecular weights, highlighting their great potential for practical application [20]. Generally speaking, the ancillary ligands exhibit a crucial influence on the catalytic activity. For example, the phenoxy-ligated half-titanocene $(\eta^5\text{-}C_5Me_5)TiCl_2(O\text{-}2,6\text{-}^iPr_2C_6H_3)$ showed high catalytic activity of 8.4×10^6 g_{PE} mol_{Ti}^{-1} h^{-1} at room temperature and 27.6×10^6 g_{PE} mol_{Ti}^{-1} h^{-1} at 140 °C for ethylene polymerization [21,22]. When the ancillary ligand is ketimide, $(\eta^5\text{-}C_5Me_5)TiCl_2(N=C^tBu_2)$ can catalyze ethylene polymerization with notable activity of 19.68×10^6 g_{PE} mol_{Ti}^{-1} h^{-1} at room temperature [21], which is two times higher than the activity achieved by the former phenoxy-ligated analogue. Furthermore, the bridged half-titanocene $[Me_2Si(\eta^5\text{-}C_5Me_4)(N^tBu)]TiCl_2$ with CGC structure also showed higher catalytic activity (33.0×10^6 g_{PE} $molTi^{-1}$ h^{-1} at 140 °C) for ethylene polymerization than the non-bridged one $(\eta^5\text{-}C_5Me_5)TiCl_2(O\text{-}2,6\text{-}^iPr_2C_6H_3)$ [22]. Despite the outstanding catalytic performances of these complexes, the influence of ancillary ligands on catalytic activity and microstructure of the polyethylene has not been investigated in detail.

Computational chemistry has been considered as a reliable tool to elucidate the mechanism of coordination polymerization recently, promoting the development of transition metal catalysts [23–28]. The mechanism of ethylene polymerization catalyzed by the non-bridged zirconocenes was systematically studied by Cundari et al. It was shown that the substituents of cyclopentadienyl or indenyl affected the kinetics and thermodynamics of reaction more significantly than the types of cyclopentadienyl ligand attached to Zr, and the substituent effects were greater than those arising from the central metal [18]. Moreover, the stronger the metal–counteranion interaction could induce the harder displacement of the counteranion by ethylene, that formed the π-complexes for chain growth [29]. By DFT study, it was found that the activation effect of metal chlorides ($MgCl_2$, $LiCl$, $ZnCl_2$, $CaCl_2$) on post-titanocene complexes for ethylene polymerization was mainly caused by the secondary complexation reaction between post-titanocene and metal chloride [30]. Marks et al. communicated the preliminary results of the ab initio computational investigation on Me_2Si-bridged Cp/amido systems and found that counteranion and solvation effects were substantial [31,32]. They also found that the ion pair $Ti\cdots H_3CB$ interaction was predominantly electrostatic in character [32]. Recently, we have been focusing on the experimental and theoretical studies on the coordination polymerization of olefins or conjugated dienes by early transition metal complexes [33–37], especially the theoretical study on mechanism of the non-bridged half-titanocene systems for polymerization of 1,7-octadiene and copolymerization of ethylene and styrene [36,37]. The ancillary ligand is a key factor in determining the selectivity; on the other hand, the chain-end of polymer can also affect the insertion.

In the present study, we focused on the reactivity of the half-titanocene-catalyzed ethylene polymerization to get insights into the roles of different ancillary groups. Thus, we report the study on the mechanisms of ethylene polymerization catalyzed by three half-titanocenes bearing different ancillary groups by DFT method. In addition, we investigated the influence of steric hindrance and electronic effect of the ancillary groups on the catalytic activity of ethylene polymerization during initiation and propagation stage that was discussed in the latter sections. Moreover, β-H transfer and the β-H elimination pathway in the termination stage were also investigated.

2. Results and Discussion

2.1. The Chain Initiation

The complexes $(\eta^5\text{-}C_5Me_5)TiCl_2(O\text{-}2,6\text{-}^iPr_2C_6H_3)$ (**1**), $(\eta^5\text{-}C_5Me_5)TiCl_2(N=C^tBu_2)$ (**2**) and $[Me_2Si(\eta^5\text{-}C_5Me_4)(N^tBu)]TiCl_2$ (**3**) could be considered to generate the alkyl titanium cations $[Cp^*Ti(O\text{-}2,6\text{-}^iPr_2C_6H_3)CH_3]^+$ (**1A**), $[Cp^*Ti(N=C^tBu_2)CH_3]^+$ (**2A**) and $[(Me_2Si(Me_4Cp)(N^tBu)TiCH_3]^+$ (**3A**), respectively, which served as the initial active species in the present computational study (Figure 1). For the process of ethylene insertion, the modified Cossee–Arlman mechanism was employed for the three active species with d^0-metal Ti^{4+} [38,39], consisting of three main steps (Figure 2): (1) the ethylene coordinates to the vacant site of

active species (**A**) to generate an ethylene π-complexes (**B**); (2) the coordinated ethylene inserts into the Ti–C(sp^3) bond through a four-center transition state **TS$_{(B-C)}$** and alkyl migration, resulting in the intermediate **C** with a γ-agostic bond; (3) and the intermediate **C** isomerizes to form the more stable complex **D** with a β-agostic bond.
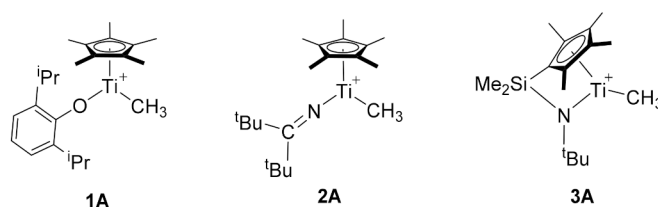

Figure 1. The proposed active species **1A**, **2A**, and **3A**.
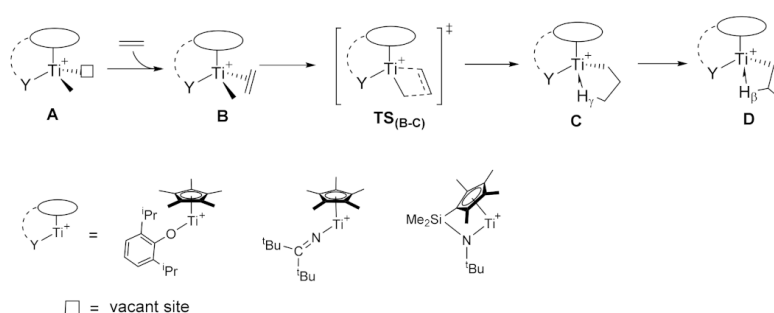

Figure 2. The proposed initiation process of ethylene polymerization initiated by half-titanocenes.

According to the proposed mechanism of initiation stage, the potential energy profiles were calculated and shown in Figure 3. With the coordination of ethylene to **1A**, **2A**, and **3A**, the corresponding π-complexes **1B**, **2B**, and **3B** were generated along with releasing energies of 9.9, 6.2, and 8.1 kcal/mol, respectively. Through the four-center transition states **1TS$_{(B–C)}$**, **2TS$_{(B–C)}$**, and **3TS$_{(B–C)}$**, the respective free energy barriers of 12.0, 10.3, and 9.2 kcal/mol had to be overcome for insertion of ethylene into **1A**, **2A**, and **3A**. The ethylene insertion pathway into the Ti−methyl bond of the {[H$_2$Si(C$_5$H$_4$)(^{t}BuN)]TiCH$_3$}$^+$ {H$_3$CB(C$_6$F$_5$)$_3$}$^-$ ion pair was also investigated by Marks et al. [40]. The computed results show an ethylene activation/insertion distal to the H$_3$CB(C$_6$F$_5$)$_3$$^-$ group in benzene is reported to be 8.0 kcal/mol, in agreement with the present DFT result for **3TS$_{(B–C)}$** in toluene of 8.1 kcal/mol. Then, the ethylene inserted intermediates **1C**, **2C**, and **3C** with γ-agostic bonds and the isomerized products **1D**, **2D**, and **3D** with β-agostic bonds were obtained exothermically (15.3–19.9 kcal/mol). It is shown that the first ethylene can be initiated successfully by the above-mentioned three model active species (**1A**, **2A**, and **3A**) as suggested by the moderate free energy barriers and the exergonic processes. Moreover, the initiation process of **1A** was kinetically less favorable among the three complexes given the highest free energy barrier.

It is known that the insertion of an alkene or alkyne molecule into a metal-C(sp^3) bond mainly involves an orbital interaction of the occupied metal-C(sp^3) bonding orbital with an unoccupied π* orbital of the alkene or alkyne, implying a nucleophilic attack of the Ti–C(sp^3) bond towards one of the alkene or alkyne carbons [41]. In other words, the incoming coordinated ethylene can be considered as an electrophile to interact with the Ti–C(sp^3) bond under this condition. The natural bond orbital (NBO) analysis was conducted in order to further explore the reason for different free energy barriers. The natural atomic charges of the sp^3 carbon bonded to Ti^{4+} were calculated to be −0.95, −0.99, and −1.00 in **1B**, **2B**, and **3B**, respectively, suggesting that the C(sp^3) atom was more electron deficient in **1B** than those in **2B** and **3B**. Therefore, the ethylene insertion transition state **1TS$_{(B–C)}$** is electronically unfavorable than **2TS$_{(B–C)}$** and **3TS$_{(B–C)}$** owing to the electron withdrawing property of the electronegative O atom in the phenoxy ligand in **1B**.
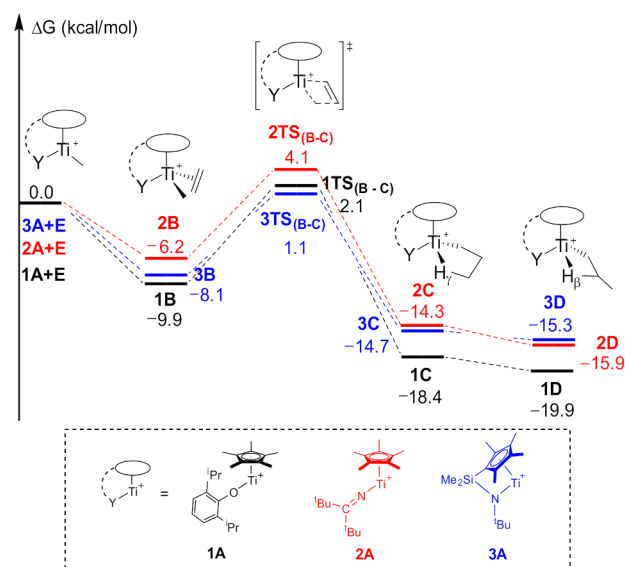
Figure 3. The calculated free energy profiles (energy in kcal/mol) for initiation stage of ethylene polymerization catalyzed by half-titanocenes.

Furthermore, the HOMO and LUMO orbitals of the ethylene coordinated intermediates **1B**, **2B**, and **3B** are shown in Figure 4. The important HOMO orbitals at **1B**, **2B**, and **3B** corresponded to the σ bonding orbital of the Ti–C(sp^3) bond, which was the bonding interaction between Ti $3d_{z^2}$ and carbon $2p_z$ orbitals. (Some occupied HOMOs of **1B**, **2B** and **3B** were shown in Figure S1 in supporting information). On the other hand, the LUMO orbitals corresponded to the π* orbitals of the ethylene molecule. Similar bonding interactions were described in a previous report [42]. The energy gap between important HOMO and LUMO orbitals in **1B** was observed to be 4.78 eV (Figure 4a), which was higher than that in **2B** of 4.58 eV (Figure 4b) and **3B** of 4.55 eV (Figure 4c). These results indicate that the interaction between the ethylene and Ti center in **1B** is the weakest.
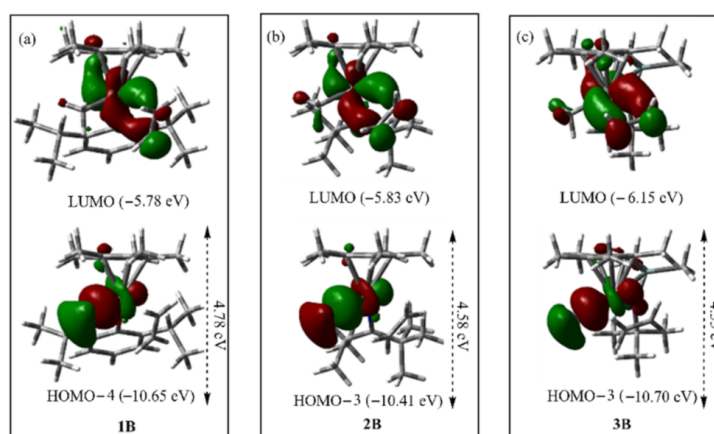

Figure 4. Important molecular orbitals at the intermediates **1B**, **2B**, and **3B**: (**a**) LUMO and HOMO-4 molecular orbitals of **1B**; (**b**) LUMO and HOMO-3 molecular orbitals of **2B**; (**c**) LUMO and HOMO-3 molecular orbitals of **3B**.

To better evaluate the different steric properties of the ancillary groups in three active species (**1A**, **2A**, and **3A**), the steric maps (contours) calculated from optimized structures of active species were compared and the buried volume %V$_{Bur}$ was also calculated (Figure 5) [43]. The %V$_{Bur}$ of **1A** is calculated to be 70.9 and the largest among three catalysts. The strong steric repulsions in active specie **1A** could account for the high free

energy barrier in the initiation process of **1A**. Additionally, the similar two ketimide is accompanied by a slight increase of the overall steric pressure of the ancillary ligand from %V_{Bur} = 64.4 for non-bridged structure in **2A** to %V_{Bur} = 66.4 for bridged CGC structure in **3A**. It is indicated the slightly larger steric repulsions, apparently attributed to the more rigid bridged cyclopentadienyl amide ligand of **3A**.
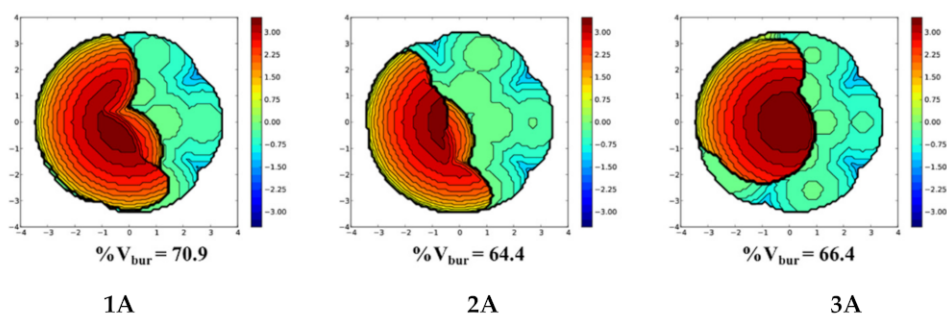

Figure 5. Topographic steric maps and the buried volume %V_{Bur} of three active species **1A**, **2A**, and **3A**. The maps were obtained starting from the minimum energy structures of complexes optimized by DFT calculations.

2.2. The Chain Propagation

In contrast to the initiation process, during chain propagation stage, the second ethylene molecule will coordinate and insert into the new active species **D** from two different directions, i.e., the front-side and back-side. The two directions are oriented according to the relative orientation of the incoming ethylene and the agostic interaction in **D** (Figure 6). Then, the insertion of the second ethylene will be achieved through the four-center transition states to obtain the complexes **F-fsi** and **F-bsi** derived respectively from front-side and back-side insertions (Figure 7). After that, the polymer chain can be generated via a similar continuous insertion process.

The free energy profiles in chain propagation process were calculated and shown in Figure 8. After initiation by **1D**, the front-side insertion was kinetically more favorable than the back-side insertion in the propagation process of complex **1** (6.8 kcal/mol for front-side insertion and 11.3 kcal/mol for back-side insertion). Similarly, it was also kinetically more favorable for the front-side insertion in the propagation process of complex **2**. On the other hand, the free energy barrier of front-side insertion (7.4 kcal/mol) was close to that of back-side insertion (7.9 kcal/mol) in the propagation process of complex **3**, suggesting that the tendencies for both side insertion directions are comparable.
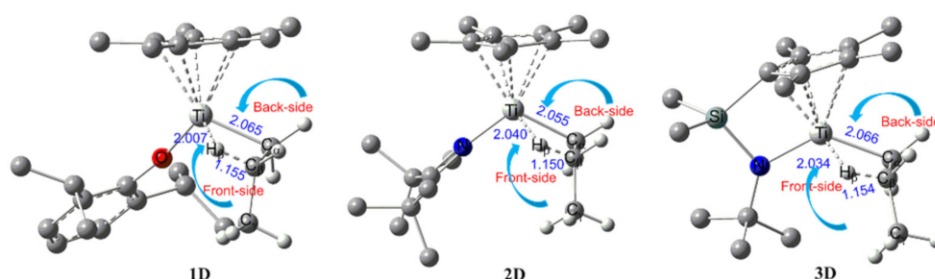

Figure 6. Optimized structures (distances in Å) of **1D**, **2D**, and **3D**. Hydrogen atoms of the Cp* ligand and ancillary ligand have been omitted for clarity.
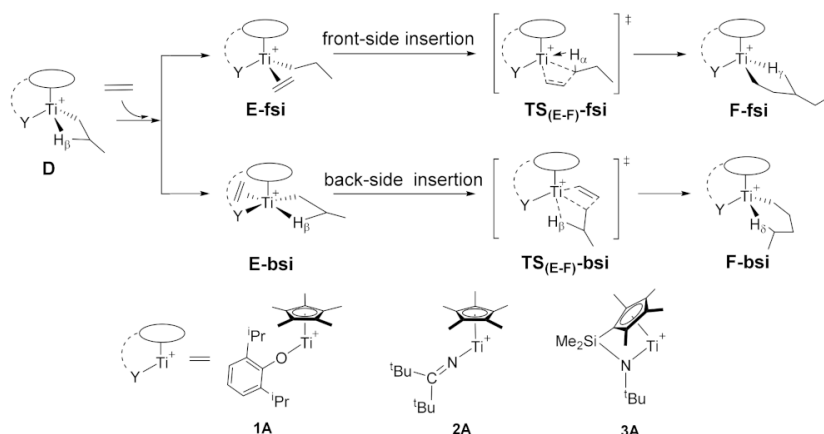
Figure 7. The proposed propagation process of ethylene polymerization catalyzed by half-titanocenes.
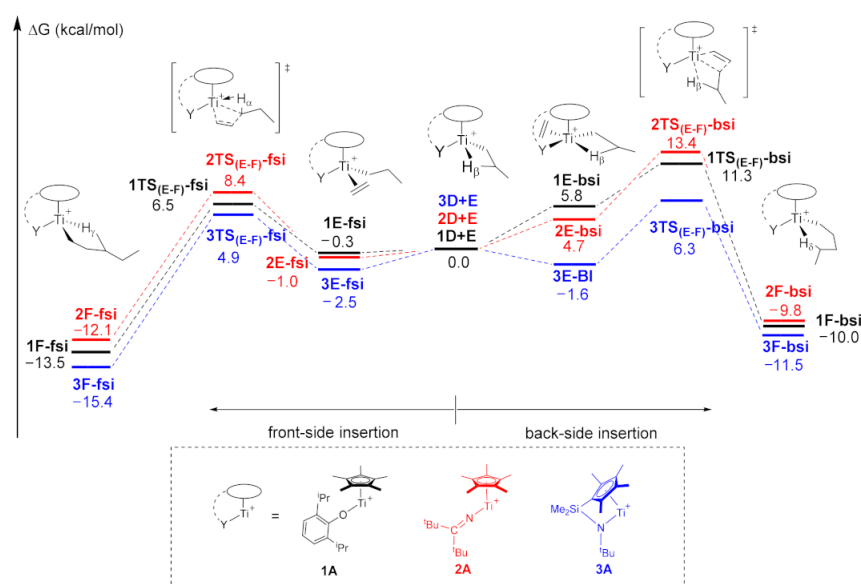

Figure 8. The calculated free energy profiles (energy in kcal/mol) for propagation stage of ethylene polymerization catalyzed by half-titanocenes.

According to the free energy profiles (Figures 3 and 8), the insertion and chain propagation of ethylene processes were exergonic, indicating that these two processes are thermodynamically favorable for all the complexes. The rate determination step in ethylene polymerization by complexes **1**–**3** was the insertion of ethylene to the initial active species **A**, having respective activation energies in initiation stage of 12.0, 10.3, and 9.2 kcal/mol for complexes **1**, **2**, and **3**. It is noted that the order of activation energy is in correspondence with the polymerization activity observed in the experimental findings [21,22].

In order to further investigate the insertion modes and stability of transition states in the propagation stage, the energy decomposition of transition states was carried out [44]. The transition states could be considered to consist of two fragments: the active species moiety (**I**) and the ethylene moiety (**II**). The single-point energy was calculated to evaluate the energy of transition state, fragments **I** and **II**, and their relationship could be evaluated according to the relation: $\Delta E_{TS} = \Delta E_{int} + \Delta E_{def}$ (**I**) + ΔE_{def} (**II**). In this expression, ΔE_{TS} represents the single-point energy of transition state. ΔE_{int} represents the interaction energy, which is estimated by the single-point energy of corresponding fragments and the energy of transition state. ΔE_{def} (**I**) and ΔE_{def} (**II**) represent the deformation energies of the two

fragments, which are estimated by the differences between the single-point energies of corresponding fragments and their energies in the optimized geometries.

The results of decomposition energy were calculated and shown in Table 1. ΔE_{int} in front-side insertions were found to be -37.0 kcal/mol for **1TS$_{(E-F)}$-fsi**, -36.0 kcal/mol for **2TS$_{(E-F)}$-fsi**, and -36.3 kcal/mol for **3TS$_{(E-F)}$-fsi**, which were higher than the ΔE_{int} in the corresponding back-side insertions (-40.3 kcal/mol for **1TS$_{(E-F)}$-bsi**, -37.5 kcal/mol for **2TS$_{(E-F)}$-bsi** and -42.7 kcal/mol for **3TS$_{(E-F)}$-bsi**). These results indicate that the interactions between active species and ethylene in back-side insertions are stronger than that in front-side insertions. The deformation energies of active species moiety (ΔE_{def} (**I**)) for **3TS** were 18.5 kcal/mol in front-side insertion and 16.4 kcal/mol in back-side insertion, which were lower than the ΔE_{def} (**I**) energies of **1TS** and **2TS** in two different directions (Table 1, entries 1–4). It is suggested that the intermediates and transition states derived from **3** are more rigid, apparently attributed to the bridged cyclopentadienyl amide ligand. Moreover, the deformation energies of ethylene ΔE_{def} (**II**) in front-side insertions were 27.3 kcal/mol for **1TS$_{(E-F)}$-fsi**, 29.6 kcal/mol for **2TS$_{(E-F)}$-fsi**, and 26.5 kcal/mol for **3TS$_{(E-F)}$-fsi**, which were all lower than those in back-side insertions (32.5 kcal/mol for **1TS$_{(E-F)}$-bsi**, 34.6 kcal/mol for **2TS$_{(E-F)}$-bsi**, and 32.1 kcal/mol for **3TS$_{(E-F)}$-bsi**). This is probably caused by the steric hindrance of the alkyl bonded to the central Ti.

Table 1. The energy decomposition (kcal/mol) of six ethylene insertion transition states in chain propagation stage.

Entry	Active Species	Insertion Direction	Transition State	ΔE_{int} (kcal/mol)	ΔE_{def} (I) (kcal/mol)	ΔE_{def} (II) (kcal/mol)	ΔE_{def} (kcal/mol) [1]
1	**1A**	front-side	**1TS$_{(E-F)}$-fsi**	-37.0	21.5	5.8	27.3
2	**1A**	back-side	**1TS$_{(E-F)}$-bsi**	-40.3	20.1	12.4	32.5
3	**2A**	front-side	**2TS$_{(E-F)}$-fsi**	-36.0	21.0	8.6	29.6
4	**2A**	back-side	**2TS$_{(E-F)}$-bsi**	-37.5	20.0	14.6	34.6
5	**3A**	front-side	**3TS$_{(E-F)}$-fsi**	-36.3	18.5	8.0	26.5
6	**3A**	back-side	**3TS$_{(E-F)}$-bsi**	-42.7	16.4	15.7	32.1

[1] $\Delta E_{def} = \Delta E_{def}$ (**I**) + ΔE_{def} (**II**).

2.3. The Chain Termination

The molecular weight of polymer material is a vital factor in determining its performance and application. It is therefore of importance to study the chain termination mechanism in order to optimize the catalyst's structure in controlling the molecular weights. Two routes can be considered in the chain termination process derived from complex **D** with a β-H agostic interaction (Figure 9) [45,46]. In one route, a direct β-H elimination occurs to generate a hydride complex (**H–E**) coordinated with one olefin molecule. In another route, a β-H transfer to ethylene occurs following the coordination of another ethylene to generate a new alkyl complex **H–T**.

The free energy profiles for two chain termination routes were calculated and shown in Figure 10. The β-H eliminations were all kinetically comparable for complexes **1**, **2** and **3**, as shown in the similar free energy barriers in the range of 15.1 to 15.7 kcal/mol. The β-H eliminations were all endergonic processes for complexes **1**, **2**, and **3**, indicating that they are thermodynamically unfavorable. Conversely, the β-H transfer could be considered to be a dominant chain termination route as suggested by the exergonic processes with 3.5, 1.5 and 6.8 kcal/mol for complexes **1**, **2**, and **3**, respectively. The free energy barrier of β-H transfer for complex **1** was higher than those for complexes **2** and **3**, which might account for the higher molecular weight of polyethylene obtained by using complex **1**. According to the calculated free energy profiles (Figures 8 and 10), the free energy barriers of β-H transfer were higher than those of chain propagation regardless of the front-side or back-side insertion. The kinetic results indicate the catalytic systems are favorable to produce the polyethylene with high molecular weights.
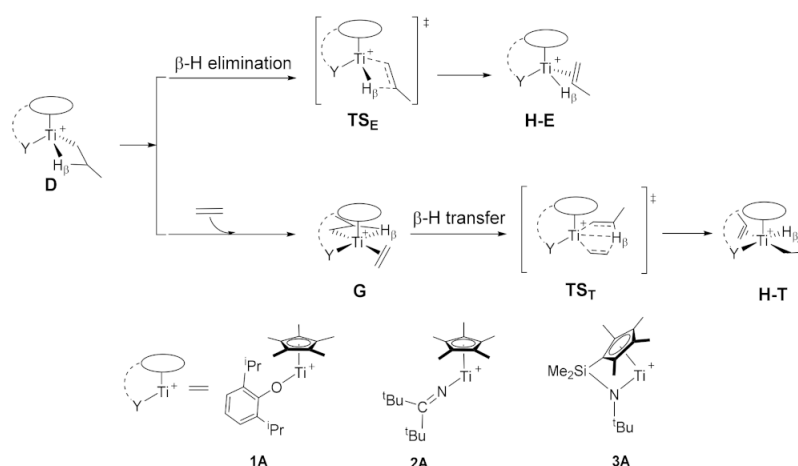
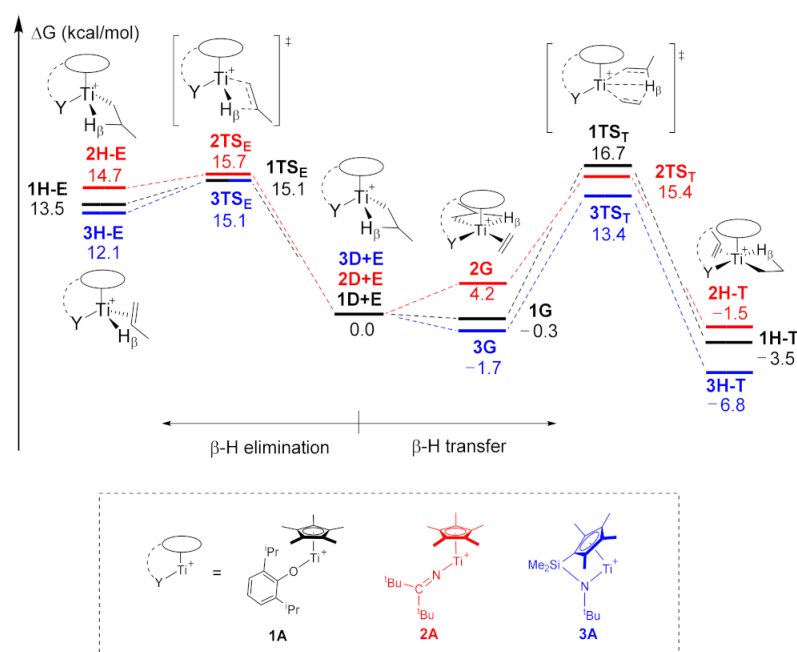**Figure 9.** The proposed termination process of ethylene polymerization catalyzed by half-titanocenes.

Figure 10. The calculated free energy profiles (energy in kcal/mol) for *β*-H elimination and *β*-H transfer in the termination stage of ethylene polymerization catalyzed by half-titanocenes.

3. Computational Details

Full geometry optimizations have been performed at the Becke3LYP (B3LYP) function of the density functional theory [47]. The effective core potentials (ECPs) of Hay and Wadt with a double-*ζ* valence basis set (LanL2DZ) [48] were used for Ti atom and a 6–31G** basis set was used for all other atoms. Frequency calculations were carried out to confirm the characteristics of all of the optimized structures as minima or transition states. Intrinsic reaction coordinate (IRC) calculations were performed on the transition states in order to confirm the expected reactants and products [49]. To obtain the relative Gibbs free energy in solution, single-point energy calculations were carried out using M06-2X functional [50] together with the polarized continuum model (PCM) [51] for considering the toluene solvation effect. The Stuttgart/Dresden effective core potential (ECP) basis set was used for Ti atom, and the larger basis set 6–311G** was used for all the other atoms. All of the DFT calculations were performed with the Gaussian 09 program [52].

4. Conclusions

The reaction mechanisms of ethylene polymerization catalyzed by three half-titanocene complexes [Cp*TiCl$_2$(O-2,6-^{i}Pr$_2$C$_6$H$_3$] (**1**) [Cp*TiCl$_2$(N=C^{t}Bu$_2$)] (**2**) and [Me$_2$Si(Me$_4$Cp)(N^{t}Bu) TiCl$_2$] (**3**) have been investigated by DFT method. Having achieved an agreement between theory and experiment, the following conclusions can be drawn. In the chain initiation, the energy profiles showed that the first ethylene insertion into the active specie **1A** was slowest among the three catalysts. The NBO analysis suggested that the electron withdrawing property of the electronegative O atom in the phenoxy ligand in **1A** made the nucleophilic attack of the Ti–C(sp^3) bond towards ethylene carbons less electronically unfavorable. The topographic steric maps and the buried volume = %V$_{Bur}$ of three active species shown the larger steric repulsions could account for the highest free energy barrier in the initiation process of **1A**. The rate determination steps for ethylene polymerizations were calculated to be the chain initiation. In the chain propagation, the ethylene front-side insertions and back-side insertions were investigated. The energy decomposition of TSs indicated the rigidity of bridged CGC structure caused the lower deformation energy in **3TS$_{(E-F)}$-bsi** and **3TS$_{(E-F)}$-fsi**. In the chain termination, the β-H transfer was calculated as the dominant chain termination route in comparison to the β-H elimination owing to the thermodynamic perspective. This study can provide further understanding on the relationship between the structure of complexes and their catalytic performance on polymerization. However, we should mention that the counter-anion of active species could also affect the coordination of ethylene to some extent [31,32,40]. And the proportions of active species in Arrhenius law, which depend on the activation conditions/nature of cocatalyst, are not in consideration in this article. Clearly, more experimental and computational studies are needed in order to have a better understanding of the ethylene polymerization reactions.

Author Contributions: Conceptualization, X.X. and Y.P.; methodology, Y.L., X.L. and X.X.; software, Y.L. and X.L.; validation, Y.D. and Z.Z.; formal analysis, Y.D.; investigation, Y.L., X.L. and X.X.; data curation, Y.L. and Y.P.; writing—original draft preparation, X.L.; writing—review and editing, Y.-M.S. and Y.P.; supervision, Y.L. and Y.P.; project administration, Y.P.; funding acquisition, Y.L. and Y.P. All authors have read and agreed to the published version of the manuscript.

Conflicts of Interest: The authors declare no conflict of interest.

References

1. Sauter, D.; Taoufik, M.; Boisson, C. Polyolefins, a Success Story. *Polymers* **2017**, *9*, 185. [CrossRef]
2. Chen, Z.; Brookhart, M. Exploring Ethylene/Polar Vinyl Monomer Copolymerizations Using Ni and Pd α-Diimine Catalysts. *Acc. Chem. Res.* **2018**, *51*, 1831–1839. [CrossRef]
3. Ma, Z.; Yang, W.; Sun, W.-H. Recent Progress on Transition Metal (Fe, Co, Ni, Ti and V) Complex Catalysts in Olefin Polymerization with High Thermal Stability. *Chin. J. Chem.* **2017**, *35*, 531–540. [CrossRef]
4. Zhang, S.; Wu, Y.-X. Controlled polymerization of olefin and its macromolecular engineering. *Sci. Sin. Chim.* **2018**, *48*, 590–600. [CrossRef]
5. Baier, M.C.; Zuideveld, M.A.; Mecking, S. Post-Metallocenes in the Industrial Production of Polyolefins. *Angew. Chem. Int. Ed.* **2014**, *53*, 9722–9744. [CrossRef]
6. Chen, C. Designing catalysts for olefin polymerization and copolymerization: Beyond electronic and steric tuning. *Nat. Rev. Chem.* **2018**, *2*, 6–14. [CrossRef]
7. Matsugi, T.; Fujita, T. High-performance olefin polymerization catalysts discovered on the basis of a new catalyst design concept. *Chem. Soc. Rev.* **2008**, *37*, 1264–1277. [CrossRef]

8. Zaccaria, F.; Budzelaar, P.H.M.; Zuccaccia, C.; Cipullo, R.; Macchioni, A.; Busico, V.; Ehm, C. Chain Transfer to Solvent and Monomer in Early Transition Metal Catalyzed Olefin Polymerization: Mechanisms and Implications for Catalysis. *Catalysts* **2021**, *11*, 215. [CrossRef]

9. Shamiri, A.; Chakrabarti, M.H.; Jahan, S.; Hussain, M.A.; Kaminsky, W.; Aravind, P.V.; Yehye, W.A. The Influence of Ziegler-Natta and Metallocene Catalysts on Polyolefin Structure, Properties, and Processing Ability. *Materials* **2014**, *7*, 5069–5108. [CrossRef] [PubMed]

10. Nomura, K. Half-Titanocenes Containing Anionic Ancillary Donor Ligands: Effective Catalyst Precursors for Ethylene/Styrene Copolymerization. *Catalysts* **2013**, *3*, 157–175. [CrossRef]

11. Nomura, K.; Naga, N.; Miki, M.; Yanagi, K. Olefin Polymerization by (Cyclopentadienyl) (aryloxy) titanium(IV) Complexes−Cocatalyst Systems. *Macromolecules* **1998**, *31*, 7588–7597. [CrossRef]

12. Nomura, K.; Naga, N.; Miki, M.; Yanagi, K.; Imai, A. Synthesis of Various Nonbridged Titanium(IV) Cyclopentadienyl−Aryloxy Complexes of the Type CpTi(OAr)X2 and Their Use in the Catalysis of Alkene Polymerization. Important Roles of Substituents on both Aryloxy and Cyclopentadienyl Groups. *Organometallics* **1998**, *17*, 2152–2154. [CrossRef]

13. Nomura, K.; Fujita, K.; Fujiki, M. Olefin polymerization by (cyclopentadienyl)(ketimide)titanium(IV) complexes of the type, $Cp'TiCl_2(N = C^tBu_2)$-methylaluminoxane (MAO) catalyst systems. *J. Mol. Catal. A Chem.* **2004**, *220*, 133–144. [CrossRef]

14. Nomura, K.; Fujita, K.; Fujiki, M. Effects of cyclopentadienyl fragment in ethylene, 1-hexene, and styrene polymerizations catalyzed by half-titanocenes containing ketimide ligand of the type, $Cp'TiCl_2(N = C^tBu_2)$. *Catal. Commun.* **2004**, *5*, 413–417. [CrossRef]

15. Stephan, D.W.; Stewart, J.C.; Guérin, F.; Spence, R.E.V.H.; Xu, W.; Harrison, D.G. Phosphinimides as a Steric Equivalent to Cyclopentadienyl: An Approach to Ethylene Polymerization Catalyst Design. *Organometallics* **1999**, *18*, 1116–1118. [CrossRef]

16. Yue, N.; Hollink, E.; Guérin, F.; Stephan, D.W. Zirconium Phosphinimide Complexes: Synthesis, Structure, and Deactivation Pathways in Ethylene Polymerization Catalysis. *Organometallics* **2001**, *20*, 4424–4433. [CrossRef]

17. Nomura, K.; Liu, J.; Padmanabhan, S.; Kitiyanan, B. Nonbridged half-metallocenes containing anionic ancillary donor ligands: New promising candidates as catalysts for precise olefin polymerization. *J. Mol. Catal. A Chem.* **2007**, *267*, 1–29. [CrossRef]

18. Nomura, K. Half-titanocenes containing anionic ancillary donor ligands as promising new catalysts for precise olefin polymerization. *Dalton Trans.* **2009**, *38*, 8811–8823. [CrossRef] [PubMed]

19. Zhao, W.; Nomura, K. Design of Efficient Molecular Catalysts for Synthesis of Cyclic Olefin Copolymers (COC) by Copolymerization of Ethylene and α-Olefins with Norbornene or Tetracyclododecene. *Catalysts* **2016**, *6*, 175. [CrossRef]

20. Nomura, K.; Liu, J. Half-titanocenes for precise olefin polymerisation: Effects of ligand substituents and some mechanistic aspects. *Dalton Trans.* **2011**, *40*, 7666–7682. [CrossRef]

21. Nomura, K.; Yamada, J.; Wei, W.; Liu, J. Effect of ketimide ligand for ethylene polymerization and ethylene/norbornene copolymerization catalyzed by (cyclopentadienyl) (ketimide) titanium complexes-MAO catalyst systems: Structural analysis for $Cp*TiCl_2(N = CPh_2)$. *J. Organomet. Chem.* **2007**, *692*, 4675–4682. [CrossRef]

22. Kim, T.J.; Kim, S.K.; Kim, B.J.; Hahn, J.S.; Ok, M.A.; Song, J.H.; Shin, D.H.; Ko, J.; Cheong, M.; Kim, J.; et al. Half-Metallocene Titanium(IV) Phenyl Phenoxide for High Temperature Olefin Polymerization: Ortho-Substituent Effect at Ancillary o-Phenoxy Ligand for Enhanced Catalytic Performance. *Macromolecules* **2009**, *42*, 6932–6943. [CrossRef]

23. Deng, L.; Margl, P.; Ziegler, T. A Density Functional Study of Nickel(II) Diimide Catalyzed Polymerization of Ethylene. *J. Am. Chem. Soc.* **1997**, *119*, 1094–1100. [CrossRef]

24. Xu, Z.; Vanka, K.; Ziegler, T. Influence of the Counterion $MeB(C_6F_5)_3^-$ and Solvent Effects on Ethylene Polymerization Catalyzed by $[(CpSiMe_2NR)TiMe]^+$: A Combined Density Functional Theory and Molecular Mechanism Study. *Organometallics* **2004**, *23*, 104–116. [CrossRef]

25. Kang, X.; Zhou, G.; Wang, X.; Qu, J.; Hou, Z.; Luo, Y. Alkyl Effects on the Chain Initiation Efficiency of Olefin Polymerization by Cationic Half-Sandwich Scandium Catalysts: A DFT Study. *Organometallics* **2016**, *35*, 913–920. [CrossRef]

26. Luo, G.; Luo, Y.; Hou, Z.; Qu, J. Intermetallic Cooperation in Olefin Polymerization Catalyzed by a Binuclear Samarocene Hydride: A Theoretical Study. *Organometallics* **2016**, *35*, 778–784. [CrossRef]

27. Liu, K.; Liu, Z.; Cheng, R.; He, X.; Liu, B. Mechanistic study on the effects of co-catalyst on ethylene polymerization over supported vanadocene catalyst. *Mol. Catal.* **2020**, *486*, 110852. [CrossRef]

28. Parveen, R.; Cundari, T.R.; Younker, J.M.; Rodriguez, G.; McCullough, L. DFT and QSAR Studies of Ethylene Polymerization by Zirconocene Catalysts. *ACS Catal.* **2019**, *9*, 9339–9349. [CrossRef]

29. Parveen, R.; Cundari, T.R.; Younker, J.M.; Rodriguez, G. Computational Assessment of Counterion Effect of Borate Anions on Ethylene Polymerization by Zirconocene and Hafnocene Catalysts. *Organometallics* **2020**, *39*, 2068–2079. [CrossRef]

30. Ustynyuk, L.Y.; Bulychev, B.M. Activation effect of metal chlorides in post-metallocene catalytic systems for ethylene polymerization: A DFT study. *J. Organomet. Chem.* **2015**, *793*, 160–170. [CrossRef]

31. Lanza, G.; Fragalà, I.L.; Marks, T.J. Highly Electrophilic Olefin Polymerization Catalysts. Counteranion and Solvent Effects on Constrained Geometry Catalyst Ion Pair Structure and Reactivity. *J. Am. Chem. Soc.* **1998**, *120*, 8257–8258. [CrossRef]

32. Lanza, G.; Fragalà, I.L.; Marks, T.J. Ligand Substituent, Anion, and Solvation Effects on Ion Pair Structure, Thermodynamic Stability, and Structural Mobility in "Constrained Geometry" Olefin Polymerization Catalysts: an Ab Initio Quantum Chemical Investigation. *J. Am. Chem. Soc.* **2000**, *122*, 12764–12777. [CrossRef]

33. Lanza, G.; Fragalà, I.L.; Marks, T.J. Energetic, Structural, and Dynamic Aspects of Ethylene Polymerization Mediated by Homogeneous Single-Site "Constrained Geometry Catalysts" in the Presence of Cocatalyst and Solvation: An Investigation at the ab Initio Quantum Chemical Level. *Organometallics* **2002**, *21*, 5594–5612. [CrossRef]

34. Pan, Y.; Zhao, A.; Li, Y.; Li, W.; So, Y.-M.; Yan, X.; He, G. Bis(oxazoline)-Derived N-Heterocyclic Carbene Ligated Rare-Earth Metal Complexes: Synthesis, Structure, and Polymerization Performance. *Dalton Trans.* **2018**, *47*, 13815–13823. [CrossRef] [PubMed]

35. Pan, Y.; Li, W.; Wei, N.-N.; So, Y.-M.; Li, Y.; Jiang, K.; He, G. Anilido-Oxazoline-Ligated Rare-Earth Metal Complexes: Synthesis, Characterization and Highly cis-1,4-Selective Polymerization of Isoprene. *Dalton Trans.* **2019**, *48*, 3583–3592. [CrossRef]

36. Li, W.; Jiang, X.; So, Y.-M.; He, G.; Pan, Y. Lutetium and Yttrium Complexes Supported by Anilido-oxazoline Ligand for Polymerization of 1,3-Conjugated Dienes and ε-Caprolactone. *New J. Chem.* **2020**, *44*, 121–128. [CrossRef]

37. Pan, Y.; Xu, X.; Wei, N.-N.; Hao, C.; Zhu, X.; He, G. DFT study on 1,7-octadiene polymerization catalyzed by a non-bridged half-titanocene system. *RSC Adv.* **2016**, *6*, 69939–69946. [CrossRef]

38. Xu, X.; He, G.; Wei, N.-N.; Hao, C.; Pan, Y. Selective Insertion in Copolymerization of Ethylene and Styrene Catalyzed by Half-Titanocene System Bearing Ketimide Ligand: A Theoretical Study. *Chin. J. Chem.* **2017**, *35*, 1731–1738. [CrossRef]

39. Cossee, P. Ziegler-Natta catalysis I. Mechanism of polymerization of α-olefins with Ziegler-Natta catalysts. *J. Catal.* **1964**, *3*, 80–88. [CrossRef]

40. Arlman, E.J. Ziegler-Natta catalysis II. Surface structure of layer-lattice transition metal chlorides. *J. Catal.* **1964**, *3*, 89–98. [CrossRef]

41. Niu, S.; Hall, M.B. Theoretical Studies on Reactions of Transition-Metal Complexes. *Chem. Rev.* **2000**, *100*, 353–405. [CrossRef] [PubMed]

42. Nomura, K.; Mitsudome, T.; Igarashi, A.; Nagai, G.; Tsutsumi, K.; Ina, T.; Omiya, T.; Takaya, H.; Yamazoe, S. Synthesis of (Adamantylimido) vanadium(V) Dimethyl Complex Containing (2-Anilidomethyl) pyridine Ligand and Selected Reactions: Exploring the Oxidation State of the Catalytically Active Species in Ethylene Dimerization. *Organometallics* **2017**, *36*, 530–542. [CrossRef]

43. Falivene, L.; Cao, Z.; Petta, A.; Serra, L.; Poater, A.; Oliva, R.; Scarano, V.; Cavallo, L. Towards the online computer-aided design of catalytic pockets. *Nat. Chem.* **2019**, *11*, 872–879. [CrossRef] [PubMed]

44. Kitaura, K.; Morokuma, K. A new energy decomposition scheme for molecular interactions within the Hartree-Fock approximation. *Int. J. Quantum Chem.* **1976**, *10*, 325–340. [CrossRef]

45. Kawamura-Kuribayashi, H.; Miyatake, T. A theoretical study of the ligand effect of thiobisphenoxytitanium complex catalyst on the catalytic activity for ethylene polymerization. *J. Organomet. Chem.* **2003**, *674*, 73–85. [CrossRef]

46. Margl, P.; Deng, L.; Ziegler, T. A Unified View of Ethylene Polymerization by d^0 and d^0f^n Transition Metals. 3. Termination of the Growing Polymer Chain. *J. Am. Chem. Soc.* **1999**, *121*, 154–162. [CrossRef]

47. Devlin, F.J.; Finley, J.W.; Stephens, P.J.; Frisch, M.J. Ab Initio Calculation of Vibrational Absorption and Circular Dichroism Spectra Using Density Functional Force Fields: A Comparison of Local, Nonlocal, and Hybrid Density Functionals. *J. Phys. Chem.* **1995**, *99*, 16883–16902. [CrossRef]

48. Hay, P.J.; Wadt, W.R. Ab initio effective core potentials for molecular calculations. Potentials for the transition metal atoms Sc to Hg. *J. Chem. Phys.* **1985**, *82*, 270–283. [CrossRef]

49. Fukui, K. The path of chemical reactions-the IRC approach. *Acc. Chem. Res.* **1981**, *14*, 363–368. [CrossRef]

50. Zhao, Y.; Truhlar, D.G. The M06 suite of density functionals for main group thermochemistry, thermochemical kinetics, noncovalent interactions, excited states, and transition elements: Two new functionals and systematic testing of four M06-class functionals and 12 other functionals. *Theor. Chem. Acc.* **2008**, *120*, 215–241.

51. Tomasi, J.; Mennucci, B.; Cammi, R. Quantum Mechanical Continuum Solvation Models. *Chem. Rev.* **2005**, *105*, 2999–3093. [CrossRef] [PubMed]

52. Frisch, M.J.; Trucks, G.W.; Schlegel, H.B.; Scuseria, G.E.; Robb, M.A.; Cheeseman, J.R.; Scalmani, G.; Barone, V.; Mennucci, B.; Petersson, G.A.; et al. *Gaussian 09, Revision D.01*; Gaussian, Inc.: Wallingford, CT, USA, 2010.